Modern radio engineering and telecommunication systems

Современные радиотехнические и телекоммуникационные системы

UDC 621.314:681.586.7:004.942
https://doi.org/10.32362/2500-316X-2023-11-4-36-48

RESEARCH ARTICLE

Analysis of the DC/DC Zeta topology converter ripples by applying its limiting continuous mathematical model

Vladimir K. Bityukov,
Alexey I. Lavrenov @,
Daniil A. Malitskiy

MIREA – Russian Technological University, Moscow, 119454 Russia
@ Corresponding author, e-mail: lavrenov@mirea.ru

Abstract

Objectives. A DC/DC Zeta topology converter represents a unipolar electronic device for converting an input positive voltage into a stabilized output voltage of the same polarity, which can be set at voltages both below and above the input voltage. The aim of this work is to analyze Zeta converter circuitry, which requires the following tasks to be solved: using Kirchhoff's Circuit Laws, obtain systems of equations describing converter operation in the phase of energy accumulation and in the phase of energy transfer; using a method proposed by A.I. Korshunov, combine the resulting systems of equations into a marginal continuous mathematical model; using expressions describing constant components of currents and voltages in Zeta converter, analyze their ripples and obtain equations for their calculation; compare the current and voltage values obtained from the continuous limiting mathematical model with the Zeta simulation results.

Methods. The tasks are solved using Kirchhoff's rules and the method for obtaining the limiting continuous mathematical model proposed by A.I. Korshunov. The results are analyzed using a circuit modelling in NI *Multisim*.

Results. It is shown that the phase coordinates of the mathematical model tend to real values of converter currents and voltages at a switching frequency of the power switch of more than 200 kHz. A strong correspondence was established between the calculated ripple values and their values obtained in the simulation (when changing the duty factor).

Conclusions. Mathematical models comprise the basis of unified calculation methods for any radio electronic circuit. The developed limiting continuous mathematical model allows a range of changes in current flowing through the choke windings and voltages on capacitor plates to be evaluated, including their maximum and minimum values for various converter parameters, such as power switch switching frequency, duty factor, element ratings, etc. Obtaining this information in turn enables the rational selection of the electronic component base of the converter.

Keywords: DC/DC converter, step-up and step-down converter, equivalent circuit, Zeta topology, converter, limiting continuous mathematical model, Kirchhoff's rules, ripple spreading

• **Submitted:** 28.12.2022 • **Revised:** 10.02.2023 • **Accepted:** 05.05.2023

For citation: Bityukov V.K., Lavrenov A.I., Malitskiy D.A. Analysis of the DC/DC Zeta topology converter ripples by applying its limiting continuous mathematical model. *Russ. Technol. J.* 2023;11(4):36–48. https://doi.org/10.32362/2500-316X-2023-11-4-36-48

Financial disclosure: The authors have no a financial or property interest in any material or method mentioned.

The authors declare no conflicts of interest.

НАУЧНАЯ СТАТЬЯ

Анализ пульсаций DC/DC-преобразователя, построенного по Zeta-топологии, с использованием его предельной непрерывной математической модели

В.К. Битюков,
А.И. Лавренов [@],
Д.А. Малицкий

МИРЭА – Российский технологический университет, Москва, 119454 Россия
[@] Автор для переписки, e-mail: lavrenov@mirea.ru

Резюме

Цели. DC/DC-преобразователь, построенный по Zeta-топологии, является униполярным электронным устройством, которое обеспечивает преобразование входного положительного напряжения в стабилизированное выходное напряжение той же полярности с возможностью его регулирования как ниже входного напряжения, так и выше. Цель работы – проанализировать схемотехнику Zeta-преобразователя. Для этого необходимо решить следующие задачи: при помощи правил Кирхгофа получить системы уравнений, описывавшие работу преобразователя в режимах накопления и передачи энергии; по методике, предложенной А.И. Коршуновым, объединить системы уравнений в предельную непрерывную математическую модель преобразователя; при помощи выражений, описывающих постоянные составляющие токов и напряжений в Zeta-преобразователе, провести анализ их пульсаций и получить уравнения для их расчета; провести сравнение полученных при помощи предельной непрерывной математической модели значений токов и напряжений с результатами моделирования Zeta-преобразователя.

Методы. Задача решена при помощи правил Кирхгофа и методики получения предельной непрерывной математической модели, предложенной А.И. Коршуновым. Результаты проанализированы с использованием схемотехнического моделирования в среде *Multisim*.

Результаты. Показано, что фазовые координаты математической модели стремятся к значениям реальных токов и напряжений преобразователя при частоте коммутации силового ключа более 200 кГц. Установлено высокое соответствие расчетных значений пульсаций и их значений, полученных при моделировании (при изменении коэффициента заполнения).

Выводы. Математические модели являются основой унифицированных методик расчета любых радиоэлектронных схем. Полученная предельная непрерывная математическая модель Zeta-преобразователя позволяет оценить диапазон изменения токов, протекающих через обмотки дросселей, и напряжений на обкладках конденсаторов, их максимальные и минимальные значения при различных параметрах преобразователя, таких как частота коммутации силового ключа, коэффициент заполнения, номиналы элементов и т.д. Эта модель позволяет выполнить рациональный подбор электронной компонентной базы преобразователя.

Ключевые слова: DC/DC-преобразователь, понижающе-повышающий преобразователь, эквивалентная схема, топология Zeta, преобразователь, предельная модель, непрерывная модель, математическая модель, правила Кирхгофа, размах пульсаций

• **Поступила:** 28.12.2022 • **Доработана:** 10.02.2023 • **Принята к опубликованию:** 05.05.2023

Для цитирования: Битюков В.К., Лавренов А.И., Малицкий Д.А. Анализ пульсаций DC/DC-преобразователя, построенного по Zeta-топологии, с использованием его предельной непрерывной математической модели. *Russ. Technol. J.* 2023;11(4):36–48. https://doi.org/10.32362/2500-316X-2023-11-4-36-48

Прозрачность финансовой деятельности: Авторы не имеют финансовой заинтересованности в представленных материалах или методах.

Авторы заявляют об отсутствии конфликта интересов.

INTRODUCTION

DC/DC converters are widely used in autonomous battery-powered devices such as unmanned aerial vehicles (UAVs), pyrometers, pacemakers, automotive electronics, robots, etc. [1–8]. Since the presence of a DC/DC converter in the power supply device determines both its mass-size parameters and efficiency, as well as the energy efficiency of the entire radio-electronic means (REM), it also affects the maximum period of autonomous operation without recharging. The complexity of manufacturing such power supply devices is also due to the tendency of autonomous devices to require stabilized low-voltage potentials. All this predetermines the need to develop specialized methods, algorithms, and design tools for DC/DC converters.

DC/DC converters implementing basic topologies of step-up, step-down, and polar inverting types [9, 10] into complex DC/DC converters—i.e., step-up and step-down (buck–boost) converters—require the development of design methods and a sufficient detail of supporting research [2, 4, 11–13].

The development of DC/DC converters, like that of other REMs, is based on appropriate mathematical models, which are the basis for the unified methodical approach to developing, designing and researching devices. Limiting continuous mathematical models of basic DC/DC converters are proposed in [9, 14–17]. However, so far, a converter for buck–boost DC/DC converters based on the Ćuk topology exists only in the form of a mathematical model [18, 19]. Meanwhile, there is no mathematical model of unipolar DC/DC converters based on Zeta topology or single-ended primary-inductor converter (SEPIC) topology. Here it should be noted that, while SEPIC, Zeta, and Ćuk converters are identical in terms of the electronic component base, they differ significantly from the schematic viewpoint.

MATHEMATICAL MODEL

A phase plane comprising a set of points of its possible states for each continuous mathematical model can be constructed to represent processes of a real device; here, a point on the phase plane represents the current state of the model and a change in the state when it moves. The trace from the representing point movement is referred to as a phase trajectory, while the point itself represents a phase coordinate. Continuity of the system means that the state of the system, i.e., the values of phase coordinates, can be established at any time.

The mathematical model of the device provides a means of obtaining the relationship between phase coordinates, which correspond to real currents and voltages of the DC/DC converter. Phase coordinates and real values of currents and voltages of the mathematical model coincide when the switching period T of the electronic switch tends to zero. Such mathematical models of key devices are commonly referred to as limiting models [14, 15].

The circuit of the unipolar Zeta converter (Fig. 1) first proposed in [12] comprises two chokes, L1 and L2, two capacitors, C1 and C2, an electronic switch VT1 typically implemented by field-effect transistor, as well as a control unit determining the transistor mode. Chokes L1 and L2 perform the function of energy storage and transfer via electromagnetic induction, while capacitor C1 is present in the circuit to separate the converter input from its output. The separating capacitor C1 is also sometimes referred to as a "flying capacitor" since it performs not only the function of separation but also the function of energy storage and transfer between sections of the converter [11, 12]. The remaining radio components perform traditional functions.

Two operation phases may be distinguished for the DC/DC converter, as well as for the majority of key devices. The first phase determines the energy storage mode, while the second determines the energy transfer mode. Thus, the mathematical model requires equivalent circuits to be constructed for each phase of the converter. Based on equivalent diagrams, systems of equations describing two operation phases are written.

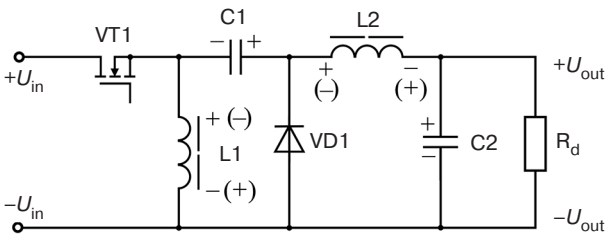

Fig. 1. Schematic diagram of the buck–boost converter based on Zeta topology. U_{in} and U_{out} are input and output voltages; R_d is the duty resistor. (In the diagrams that follow, the designations adopted in the GOST 2.710-81[1] standard are used.)

In [20], only the mathematical model of the converter with the same chokes L1 and L2 is presented. Therefore, it makes sense to construct a mathematical model of the buck–boost DC/DC converter based on Zeta topology, but in a general form.

The system of equations describing both operation phases are made according to Kirchhoff's rules. The DC/DC converter in the energy storage mode (first phase) is described by five equations of algebraic sums of currents and voltages, as follows:

[1] GOST 2.710-81. *Unified system for design documentation. Alpha-numerical designations in electrical diagrams*. Moscow: Standartinform; 2008 (in Russ.).

$$i_{in} - i_{L1} - i_{L2} = 0, \quad (1)$$

$$\begin{cases} \dfrac{du_{C2}}{dt} = \dfrac{1}{C_2} i_{L2} - \dfrac{1}{R_d C_2} u_{C2}, \\ \dfrac{du_{C1}}{dt} = \dfrac{1}{C_1} i_{L2}, \\ \dfrac{di_{L1}}{dt} = \dfrac{1}{L_1} U_{in} - \dfrac{r_1}{L_1} i_{L1}, \\ \dfrac{di_{L2}}{dt} = -\dfrac{1}{L_2} u_{C1} - \dfrac{1}{L_2} u_{C2} - \dfrac{r_2}{L_2} i_{L2} - \dfrac{1}{L_2} U_{in}, \end{cases} \quad (2)$$

where L_1 is the inductance of a choke L1; L_2 is the inductance of a choke L2; C_1 is the capacitance of a capacitor C1; C_2 is the capacitance of a capacitor C2; R_d is the resistance of a duty resistor R_d; i_{L1} and i_{L2} are instantaneous currents flowing through the winding of chokes L1 and L2; r_1 and r_2 are active resistances of the L1 and L2 choke windings; and u_{C1} and u_{C2} are instantaneous voltages at the coatings of capacitors C1 and C2.

Equation (1) containing input current i_{in}, according to Kirchhoff's rules, is necessary for describing the first phase of the inverter operation in detail. However, considering the equations of system (2) not depending on the input current, Eq. (1) can be excluded from the system.

The system of equations determining the inverter operation in the energy transfer mode (second phase) may be written as follows:

$$\begin{cases} \dfrac{du_{C2}}{dt} = \dfrac{1}{C_2} i_{L2} - \dfrac{1}{R_d C_2} u_{C2}, \\ \dfrac{du_{C1}}{dt} = \dfrac{1}{C_1} i_{L1}, \\ \dfrac{di_{L1}}{dt} = -\dfrac{r_1}{L_1} i_{L1} - \dfrac{1}{L_1} u_{C1}, \\ \dfrac{di_{L2}}{dt} = -\dfrac{r_2}{L_2} i_{L2} - \dfrac{1}{L_2} u_{C2}. \end{cases} \quad (3)$$

For building the mathematical model, it is necessary to combine systems of Eqs. (2)–(3) according to the method [14, 15]. The mathematical model may be written as the following matrix system of equations:

$$\mathbf{X} = \begin{bmatrix} i_{L1} \\ i_{L2} \\ u_{C1} \\ u_{C2} \end{bmatrix}, \quad (4)$$

$$\mathbf{A} = \begin{bmatrix} -\dfrac{r_1}{L_1} & 0 & -(1-D)\dfrac{1}{L_1} & 0 \\ 0 & -\dfrac{r_2}{L_2} & -D\dfrac{1}{L_2} & -\dfrac{1}{L_2} \\ (1-D)\dfrac{1}{C_1} & D\dfrac{1}{C_1} & 0 & 0 \\ 0 & \dfrac{1}{C_2} & 0 & -\dfrac{1}{RC_2} \end{bmatrix}, \quad (5)$$

$$\mathbf{B} = \begin{bmatrix} D\dfrac{1}{L_1} \\ -D\dfrac{1}{L_2} \\ 0 \\ 0 \end{bmatrix}, \quad (6)$$

where **X** is the matrix of the system phase coordinates; **A** is the coefficient matrix of the phase coordinates; **B** is the coefficient matrix of an external source, such as the input voltage; **D** is the fill factor of the pulse-width modulated signal controlling by power switch VT1.

Thus, the system of Eqs. (4)–(6) is the limiting continuous mathematical model of DC/DC converter based on Zeta topology.

Instantaneous currents and voltages contain constant and variable (called ripple) components. Analysis of the mathematical model shows that it would be advisable to determine separately the constant components of currents I_{L1}, I_{L2}, voltages U_{C1}, U_{C2}, and their ripples.

Solving the system of Eqs. (4)–(6) of the mathematical model for the constant components of currents I_{L1}, I_{L2} and voltages U_{C1}, U_{C2}, the following equations may be written:

$$I_{L1} = \left| \frac{U_{in} D^2}{R_d D^2 - (r_1 + 2R_d) D + R_d} \right|, \quad (7)$$

$$I_{L2} = \left| \frac{U_{in} D(D-1)}{R_d D^2 - (r_1 + 2R_d) D + R_d} \right|, \quad (8)$$

$$U_{C1} = \left| \frac{R_d U_{in} D(D-1)}{R_d D^2 - (r_1 + 2R_d) D + R_d} \right|, \quad (9)$$

$$U_{C2} = \left| -\frac{U_{in} D((r_2 + r_1 + R_d) D - (r_2 + R_1))}{R_d D^2 - (r_1 + 2R_d) D + R_d} \right|. \quad (10)$$

Using Eqs. (1), (7), and (8), the following equation for the constant component of the input current I_{in} may be written:

$$I_{in} = \left(\left| \frac{U_{in} D^2}{R_d D^2 - (r_1 + 2R_d)D + R_d} \right| + \left| \frac{U_{in} D(D-1)}{R_d D^2 - (r_1 + 2R_d)D + R_d} \right| \right) D. \quad (11)$$

Equations (7)–(11) are the basis for the preliminary calculation of the converter and hence for the selection of its electronic component base.

CURRENT AND VOLTAGE RIPPLES

Instantaneous currents i_{L1} and i_{L2} flowing through the windings of chokes L1 and L2 as well as instantaneous voltages u_{C1} and u_{C2} on capacitors C1 and C2 contain constant and variable components

$$\begin{aligned} i_{L1} &= I_{L1} + \delta i_{L1}, \quad u_{C1} = U_{C1} + \delta u_{C1}, \\ i_{L2} &= I_{L2} + \delta i_{L2}, \quad u_{C2} = U_{C2} + \delta u_{C2}, \end{aligned} \quad (12)$$

where δi_{L1} is the variable component of current i_{L1}; δi_{L2} is the variable component of current i_{L2}; δu_{C1} is the variable component of voltage u_{C1}; δu_{C2} is the variable component of voltage u_{C2}.

Substituting (12) into the systems of Eqs. (2) and (3), which describe both phases of the converter operation, the following may be written:

$$\begin{cases} \dfrac{d\left(I_{L1} + \delta i_{L1}\right)}{dt} = \dfrac{1}{L_1} U_{in} - \dfrac{r_1}{L_1}\left(I_{L1} + \delta i_{L1}\right), & (13.1) \\ \dfrac{d\left(I_{L2} + \delta i_{L2}\right)}{dt} = -\dfrac{1}{L_2}\left(U_{C1} + \delta u_{C1}\right) - \dfrac{1}{L_2}\left(U_{C2} + \delta u_{C2}\right) - \dfrac{r_2}{L_2}\left(I_{L2} + \delta i_{L2}\right) - \dfrac{1}{L_2} U_{in}, & (13.2) \\ \dfrac{d\left(U_{C1} + \delta u_{C1}\right)}{dt} = \dfrac{1}{C_1}\left(I_{L2} + \delta i_{L2}\right), & (13.3) \\ \dfrac{d\left(U_{C2} + \delta u_{C2}\right)}{dt} = \dfrac{1}{C_2}\left(I_{L2} + \delta i_{L2}\right) - \dfrac{1}{R_d C_2}\left(U_{C2} + \delta u_{C2}\right). & (13.4) \end{cases} \quad (13)$$

$$\begin{cases} \dfrac{d\left(I_{L1} + \delta i_{L1}\right)}{dt} = -\dfrac{r_1}{L_1}\left(I_{L1} + \delta i_{L1}\right) - \dfrac{1}{L_1}\left(U_{C1} + \delta u_{C1}\right), & (14.1) \\ \dfrac{d\left(I_{L2} + \delta i_{L2}\right)}{dt} = -\dfrac{r_2}{L_2}\left(I_{L2} + \delta i_{L2}\right) - \dfrac{1}{L_2}\left(U_{C2} + \delta u_{C2}\right), & (14.2) \\ \dfrac{d\left(U_{C1} + \delta u_{C1}\right)}{dt} = \dfrac{1}{C_1}\left(I_{L1} + \delta i_{L1}\right), & (14.3) \\ \dfrac{d\left(U_{C2} + \delta u_{C2}\right)}{dt} = \dfrac{1}{C_2}\left(I_{L2} + \delta i_{L2}\right) - \dfrac{1}{R_d C_2}\left(U_{C2} + \delta u_{C2}\right). & (14.4) \end{cases} \quad (14)$$

Given that $\dfrac{U_{C2}}{R_d} \approx I_{L2}$, Eqs. (13.4) and (14.4) may be simplified, as follows:

$$\frac{d\left(U_{C2} + \delta u_{C2}\right)}{dt} \approx \frac{1}{C_2}\delta i_{L2} - \frac{1}{R_d C_2}\delta u_{C2}.$$

The constant components of currents and voltages are usually much larger than the ripple, so in the right-hand sides of Eqs. (13.1)–(13.3) and (14.1)–(14.3), the ripple can be neglected compared to the corresponding constant components:

$$\begin{cases} \dfrac{d\delta i_{L1}}{dt} = \dfrac{1}{L_1}U_{in} - \dfrac{r_1}{L_1}I_{L1}, \quad (15.1) \\ \dfrac{d\delta i_{L2}}{dt} = -\dfrac{1}{L_2}U_{C1} - \dfrac{1}{L_2}U_{C2} - \dfrac{r_2}{L_2}I_{L2} - \dfrac{1}{L_2}U_{in}, \quad (15.2) \\ \dfrac{d\delta u_{C1}}{dt} = \dfrac{1}{C_1}I_{L2}, \quad (15.3) \\ \dfrac{d\delta u_{C2}}{dt} = \dfrac{1}{C_2}\delta i_{L2} - \dfrac{1}{R_d C_2}\delta u_{C2}. \quad (15.4) \end{cases} \tag{15}$$

$$\begin{cases} \dfrac{d\delta i_{L1}}{dt} = -\dfrac{r_1}{L_1}I_{L1} - \dfrac{1}{L_1}U_{C1}, \quad (16.1) \\ \dfrac{d\delta i_{L2}}{dt} = -\dfrac{r_2}{L_2}I_{L2} - \dfrac{1}{L_2}U_{C2}, \quad (16.2) \\ \dfrac{d\delta u_{C1}}{dt} = \dfrac{1}{C_1}I_{L1}, \quad (16.3) \\ \dfrac{d\delta u_{C2}}{dt} = \dfrac{1}{C_2}\delta i_{L2} - \dfrac{1}{R_d C_2}\delta u_{C2}. \quad (16.4) \end{cases} \tag{16}$$

Using Eqs. (15.1)–(15.3), the following equations for variable component (ripple) δi_{L1}, δi_{L2}, and δu_{C1} of the first phase may be written:

$$\delta i_{L1} = \int\left(\frac{1}{L_1}U_{in} - \frac{r_1}{L_1}I_{L1}\right)dt = \left(\frac{1}{L_1}U_{in} - \frac{r_1}{L_1}I_{L1}\right)t, \tag{17}$$

$$\delta i_{L2} = \int\left(-\frac{1}{L_2}U_{C1} - \frac{1}{L_2}U_{C2} - \frac{r_2}{L_2}I_{L2} - \frac{1}{L_2}U_{in}\right)dt = \left(-\frac{1}{L_2}U_{C1} - \frac{1}{L_2}U_{C2} - \frac{r_2}{L_2}I_{L2} - \frac{1}{L_2}U_{in}\right)t, \tag{18}$$

$$\delta u_{C1} = \int\left(\frac{1}{C_1}I_{L2}\right)dt = \left(\frac{1}{C_1}I_{L2}\right)t. \tag{19}$$

Using Eqs. (16.1)–(16.3), the following equations for variable components δi_{L1}, δi_{L2}, and δu_{C1} of the second phase may be written:

$$\delta i_{L1} = \int\left(-\frac{r_1}{L_1}I_{L1} - \frac{1}{L_1}U_{C1}\right)dt = \left(-\frac{r_1}{L_1}I_{L1} - \frac{1}{L_1}U_{C1}\right)t, \tag{20}$$

$$\delta i_{L2} = \int\left(-\frac{r_2}{L_2}I_{L2} - \frac{1}{L_2}U_{C2}\right)dt = \left(-\frac{r_2}{L_2}I_{L2} - \frac{1}{L_2}U_{C2}\right)t, \tag{21}$$

$$\delta u_{C1} = \int\left(\frac{1}{C_1}I_{L1}\right)dt = \left(\frac{1}{C_1}I_{L1}\right)t. \tag{22}$$

Equations (15.4) and (16.4) have the same form, so they may be written as follows:

$$\frac{d\delta u_{C2}}{dt} = y' = px - qy, \tag{23}$$

where $q = \dfrac{1}{R_d C_2}$, coefficient p is expressed by the equation

$$p_1 = \frac{1}{C_2}\left(-\frac{1}{L_2}U_{C1} - \frac{1}{L_2}U_{C2} - \frac{r_2}{L_2}I_{L2} - \frac{1}{L_2}U_{in}\right)$$

for the first phase and $p_2 = \dfrac{1}{C_2}\left(-\dfrac{r_2}{L_2}I_{L2} - \dfrac{1}{L_2}U_{C2}\right)$ for the second phase.

Solving differential Eq. (23), the following equations may be written:

$$y = \left(\frac{p(qx-1)e^{qx}}{q^2} + K\right)e^{-qx} \text{ or}$$

$$\delta u_{C2} = -\frac{p}{q^2} + \frac{pt}{q} + Ke^{-qt}. \tag{24}$$

For simplifying calculations, the boundary condition $y(0) = 0$ may be taken. Equations of constants for the first and second phases are written as follows:

$$K_1 = \frac{p_1}{q^2} \text{ and } K_2 = \frac{p_2}{q^2}. \tag{25}$$

Using Eqs. (17)–(19), the following equations for determining the ripple spreading Δi_{L1}, Δi_{L2}, and Δu_{C1} of the first phase may be written:

$$\Delta i_{L1} = \delta i_{L1}(TD) - \delta i_{L1}(0) = \left(\frac{1}{L_1}U_{in} - \frac{r_1}{L_1}I_{L1}\right)TD = -\frac{U_{in}DT\left(\left(r_1 - R_d\right)D^2 + \left(r_1 + 2R_d\right)D - R_d\right)}{L_1\left(R_d D^2 - \left(r_1 + 2R_d\right)D + R_d\right)}, \tag{26}$$

$$\Delta i_{L2} = \delta i_{L2}(TD) - \delta i_{L2}(0) = \left(-\frac{1}{L_2}U_{C1} - \frac{1}{L_2}U_{C2} - \frac{r_2}{L_2}I_{L2} - \frac{1}{L_2}U_{in}\right)TD = \frac{U_{in}DT\left(\left(r_1 - R_d\right)D^2 + \left(r_1 + 2R_d\right)D - R_d\right)}{L_2\left(R_dD^2 - \left(r_1 + 2R_d\right)D + R_d\right)}, \quad (27)$$

$$\Delta u_{C1} = \delta u_{C1}(TD) - \delta u_{C1}(0) = \left(\frac{1}{C_1}I_{L2}\right)TD = \frac{U_{in}D^2T\left(D-1\right)}{C_1\left(R_dD^2 - \left(r_1 + 2R_d\right)D + R_d\right)}. \quad (28)$$

Using Eqs. (20)–(22), the equations for determining the ripple spreading Δi_{L1}, Δi_{L2}, and Δu_{C1} of the second phase may be written:

$$\Delta i_{L1} = \delta i_{L1}(TD) - \delta i_{L1}(T) = \left(-\frac{r_1}{L_1}I_{L1} - \frac{1}{L_1}U_{C1}\right)T(1-D) = -\frac{U_{in}DT(1-D)\left(\left(r_1 + R_d\right)D - R_d\right)}{L_1\left(R_dD^2 - \left(r_1 + 2R_d\right)D + R_d\right)}, \quad (29)$$

$$\Delta i_{L2} = \delta i_{L2}(TD) - \delta i_{L2}(T) = \left(-\frac{r_2}{L_2}I_{L2} - \frac{1}{L_2}U_{C2}\right)T(1-D) = \frac{U_{in}DT(1-D)\left(\left(r_1 + R_d\right)D - R_d\right)}{L_2\left(R_dD^2 - \left(r_1 + 2R_d\right)D + R_d\right)}, \quad (30)$$

$$\Delta u_{C1} = \delta u_{C1}(TD) - \delta u_{C1}(T) = \left(\frac{1}{C_1}I_{L1}\right)T\left(D-1\right) = \frac{U_{in}D^2T\left(D-1\right)}{C_1\left(R_dD^2 - \left(r_1 + 2R_d\right)D + R_d\right)}. \quad (31)$$

Considering that the equations for determining the current ripple spreading Δi_{L1} and Δi_{L2} both are different in two phases and are equivalent, it would be advisable to determine the average ripple spreading Δi_{L1av} and Δi_{L2av} of currents flowing through the choke windings:

$$\Delta i_{L1av} = \frac{\left|-\frac{U_{in}DT\left(\left(r_1 - R_d\right)D^2 + \left(r_1 + 2R_d\right)D - R_d\right)}{L_1\left(R_dD^2 - \left(r_1 + 2R_d\right)D + R_d\right)}\right|}{2} + \frac{\left|-\frac{U_{in}DT(1-D)\left(\left(r_1 + R_d\right)D - R_d\right)}{L_1\left(R_dD^2 - \left(r_1 + 2R_d\right)D + R_d\right)}\right|}{2}, \quad (32)$$

$$\Delta i_{L2av} = \frac{\left|\frac{U_{in}DT\left(\left(r_1 - R_d\right)D^2 + \left(r_1 + 2R_d\right)D - R_d\right)}{L_2\left(R_dD^2 - \left(r_1 + 2R_d\right)D + R_d\right)}\right|}{2} + \frac{\left|\frac{U_{in}DT(1-D)\left(\left(r_1 + R_d\right)D - R_d\right)}{L_2\left(R_dD^2 - \left(r_1 + 2R_d\right)D + R_d\right)}\right|}{2}. \quad (33)$$

Using Eq. (24), the following equation for determining the ripple spreading Δu_{C2} may be written:

$$\Delta u_{C2} = \left|\delta u_{C21}\left(\frac{TD}{2}\right)\right| + \left|\delta u_{C22}\left(T\frac{1-D}{2}\right)\right| = -\frac{p_1}{q^2} + \frac{p_1\frac{TD}{2}}{q^2} + K_1e^{-q\frac{TD}{2}} - \frac{p_2}{q^2} + \frac{p_2T\frac{1-D}{2}}{q^2} + K_2e^{-qT\frac{1-D}{2}} = \frac{1}{2}\left(\left|\frac{R_dU_{in}D\left(\left(r_1 + R_d\right)D - R_d\right)}{L_2\left(R_dD^2 - \left(r_1 + 2R_d\right)D + R_d\right)}\times\left(2R_dC_2e^{\frac{T(D-1)}{2R_dC_2}} + \left((1-D)T - 2R_dC_2\right)\right)\right| + \left|\frac{R_dU_{in}D\left(\left(r_1 + R_d\right)D - R_d\right)}{L_2\left(R_dD^2 - \left(r_1 + 2R_d\right)D + R_d\right)}\times\left(2R_dC_2e^{\frac{-TD}{2R_dC_2}} + \left(DT - 2R_dC_2\right)\right)\right|\right), \quad (34)$$

where δu_{C21} is the function of the voltage ripple variable component on the capacitor C2 obtained by solving the differential equation in the first phase; δuC_{22} is the function of the voltage ripple variable component on the capacitor C2 obtained by solving the differential equation in the second phase.

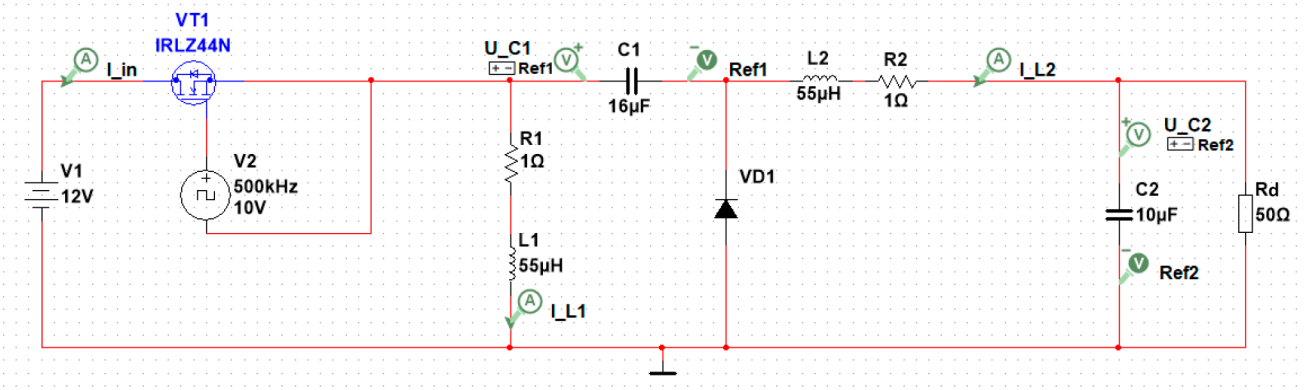

Fig. 2. Simulation scheme of the DC/DC converter

Using Eqs. (1), (32), and (33), we can write the following equation for determining the ripple spreading of input current Δi_{in}:

$$\Delta i_{in} = \frac{\Delta i_{L1av} + \Delta i_{L2av}}{2} + \frac{1}{D} I_{in} =$$
$$= \frac{1}{4}\left(\left| -\frac{U_{in} DT\left((r_l - R_d)D^2 + (r_l + 2R_d)D - R_d\right)}{L_1\left(R_d D^2 - (r_l + 2R_d)D + R_d\right)} \right| + \right.$$
$$+ \left| -\frac{U_{in} DT(1-D)\left((r_l + R_d)D - R_d\right)}{L_1\left(R_d D^2 - (r_l + 2R_d)D + R_d\right)} \right| +$$
$$+ \left| \frac{U_{in} DT\left((r_l - R_d)D^2 + (r_l + 2R_d)D - R_d\right)}{L_2\left(R_d D^2 - (r_l + 2R_d)D + R_d\right)} \right| + \quad (35)$$
$$+ \left. \left| \frac{U_{in} DT(1-D)\left((r_l + R_d)D - R_d\right)}{L_2\left(R_d D^2 - (r_l + 2R_d)D + R_d\right)} \right| \right) +$$
$$+ \left(\left| \frac{U_{in} \cdot D^2}{R_d \cdot D^2 - (r_l + 2 \cdot R_d) \cdot D + R_d} \right| + \right.$$
$$+ \left. \left| \frac{U_{in} \cdot D \cdot (D-1)}{R_d \cdot D^2 - (r_l + 2 \cdot R_d) \cdot D + R_d} \right| \right).$$

Thus, Eqs. (28) or (31) and (32)–(35) allow calculating the ripple spreading of currents i_{L1}, i_{L2} flowing through the windings of chokes L1 and L2, input current i_{in} and voltages u_{C1}, u_{C2} at the coatings of capacitors C1 and C2, if the nominal values of selected electronic components and the converter operating mode (duty factor D and period T) are known.

SIMULATION IN THE *MULTISIM* ENVIRONMENT

For checking the validity of the obtained expressions for determining the ripple currents and voltages of the DC/DC converter based on Zeta topology, circuit simulation in the *Multisim*[2] environment is used. The derivation of analytical formulas and the results of simulating constant components of currents and voltages of the considered converter are presented in [20–22].

The simulation is preceded by the study of MOSFET power switches, as recommended in [23, 24], in static and dynamic mode. On this basis, the IRLZ44N transistor, whose model characteristics correspond to the Datasheet[3] data, was selected.

In the simulation scheme depicted in Fig. 2, the switch VT1 commutes the current of the input power supply V1 with the frequency of the clock pulses set by generator V2. Components from the *Multisim* database are selected as elements. The chokes are represented by equivalent circuits. The active resistance of the choke having an inductance of 55 µH does not exceed 1 Ohm.

To study the impact of the duty factor D on ripples, the circuit is simulated in the transient analysis mode. Here, the current and voltage ripples are recorded in the steady-state mode 5–12 ms after the simulation has started. The study results of the impact of duty factor D as the main parameter determining the converter operation mode are shown in Figs. 3–5. The impact of switching frequency f on the ripple spreading value is shown in Figs. 6–8.

The studies of the impact of duty factor D on the ripple spreading value show a good coincidence of the results of the mathematical model and simulation. However, at duty factors D less than 0.3 and greater than 0.7, a significant difference is observed. This discrepancy is caused by imperfection of mathematical model and impact of parasitic parameters of radio components on converter operation. The coincidence of calculated ripple spreading Δi_{in}, Δi_{Lav}, and Δu_C along with values

[2] https://www.ni.com/ru-ru.html. Accessed March 27, 2023 (in Russ.).

[3] International rectifier, IRFZ44N HEXFET Power MOSFET, Data Sheet. https://static.chipdip.ru/lib/158/DOC000158617.pdf. Accessed March 27, 2023.

Δi_{inm}, Δi_{Lm}, and Δu_{Cm} obtained during simulation is observed at duty factor D equal to 0.5. Here, Δi_{inm} is input current ripple spreading obtained by simulation; Δi_{Lm} is the ripple spreading of current flowing through winding of chokes L1 and L2 obtained by simulation; Δu_{Cm} is the voltage ripple spreading on capacitors C1 and C2 obtained by simulation. The difference between calculated values and simulation results for input current ripple is 6 mA at Δi_{in} = 718 mA. The difference between calculated values and simulation results for current ripple i_{L1}, i_{L2} is 7 mA at Δi_{Lav} = 218 mA. The difference between calculated values and simulation results is 0.3 mV at Δu_{C1} = 15 mV and 0.05 mV at Δu_{C2} = 5.45 mV for voltage ripple spreading Δu_{C1} and Δu_{C2}, respectively.

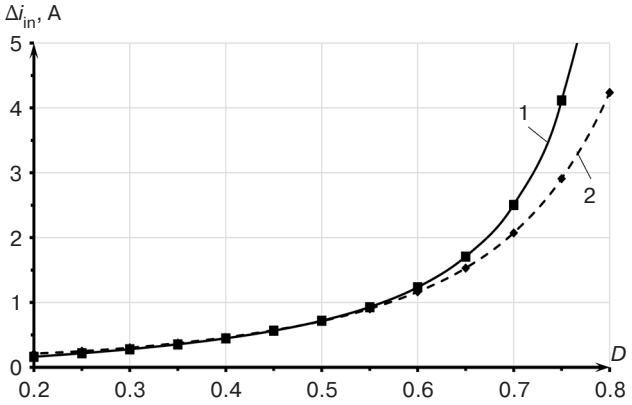

Fig. 3. Impact of the duty factor on the input current ripple: 1 is the calculated value Δi_{in}; 2 is the simulation result Δi_{inm}

From Fig. 3 it can be seen that the calculated value of input current ripple corresponds to the simulation results across almost the whole variation range of duty factor D. However, the calculation and simulation results differ at duty factors $D < 0.25$ and $D > 0.75$. This is especially evident at a duty factor D greater than 0.75. For example, at duty factor D = 0.8, the difference of calculated and simulated ripple is ~4 A at Δi_{in} = 4.3 A while at duty factor D = 0.2, this difference is ~48 mA at Δi_{in} = 163 mA.

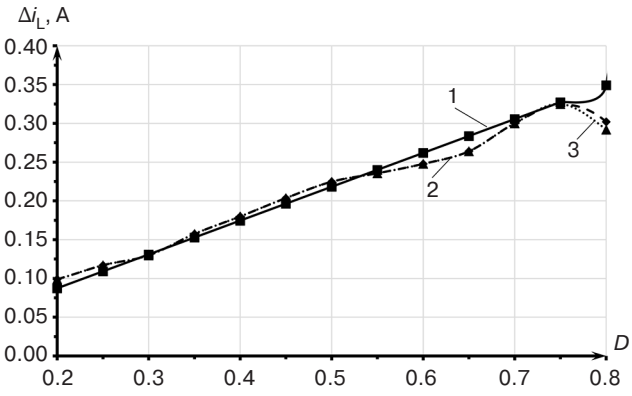

Fig. 4. Impact of the duty factor on ripple currents flowing through windings of chokes L1 and L2: 1 is the calculated value Δi_L; 2 is the simulation result Δi_{L1m}; 3 is the simulation result Δi_{L2m}

Figure 4 shows that the ripple currents flowing through the choke windings practically coincide. The calculation and simulation results, as well as in case of input current, differ systematically at duty factor $D < 0.25$ and $D > 0.75$. At duty factor D = 0.8, the difference of calculated and simulated ripple values is ~47 mA at Δi_L = 349 mA while at duty factor D = 0.2, this difference is ~13 mA at Δi_L = 87 mA.

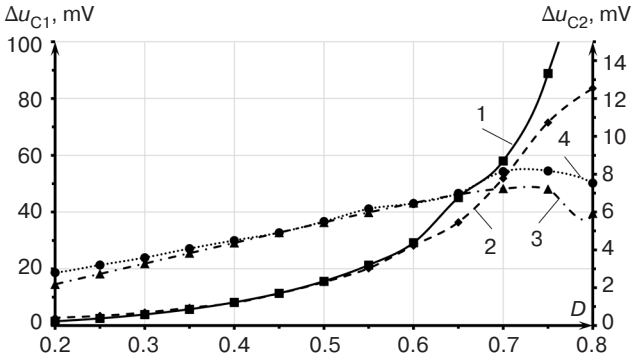

Fig. 5. Impact of the duty factor on the voltage ripple at capacitors C1 and C2: 1 is the calculated value Δu_{C1}; 2 is the simulation result Δu_{C1m}; 3 is the calculated value Δu_{C2}; 4 is the simulation result Δu_{C2m}

It follows from Fig. 5 that at duty factor of 0.5, the calculated ripples and simulation results coincide. However, the voltage ripple on capacitor C2 differs by 1.59 mV at 6 mV if D = 0.8, and by 0.6 mV at Δu_{C2} = 2.2 mV if D = 0.2.

The difference between calculated voltage value Δu_{C1} on capacitor C1 and simulation result Δu_{C1m} reaches 76 mV at Δu_{C1} = 160 mV if D ~ 0.8; however, the difference between the calculation and simulation results would be insignificant at D ~ 0.2.

When the switching frequency of the power transistor is increased, the ripple currents and voltages are significantly reduced. As shown in Fig. 6, the calculated ripple values Δi_{in} and simulation results Δi_{inm} coincide at switching frequencies from 50 to 800 kHz. The maximum difference of the calculated ripples and simulation in the operating frequency band is observed at the frequency of 50 kHz (in the enlarged scale, the difference is shown in the inset of Fig. 7) and is 0.35 A at Δi_{in} = 4.2 A.

It is shown in Fig. 7 that calculated ripple Δi_L and simulated ripple Δi_{Lm}, as well as the input current, coincide at switching frequencies from 50 to 800 kHz. The maximum difference between the calculated ripple and simulated ripple in the operating frequency band is observed at 50 kHz (in the enlarged scale, the difference is shown in the inset of Fig. 7) and is 0.26 A for Δi_{L1} and 0.2 A for Δi_{L2} at Δi_L = 2.18 A.

The limit of the continuous mathematical model is clearly visible in Fig. 8, in contrast to Fig. 7. For

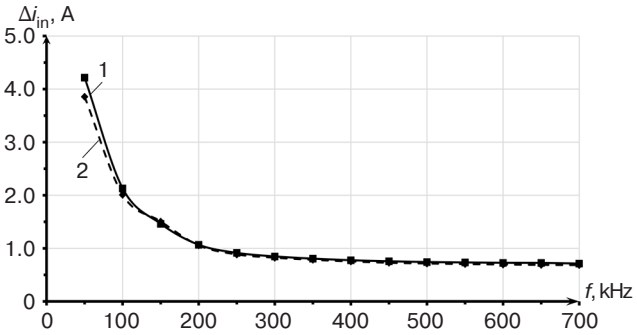

Fig. 6. Impact of switching frequency on the input current ripple at the duty factor equal to 0.5: 1 is the calculated value Δi_{in}; 2 is the simulation result Δi_{inm}

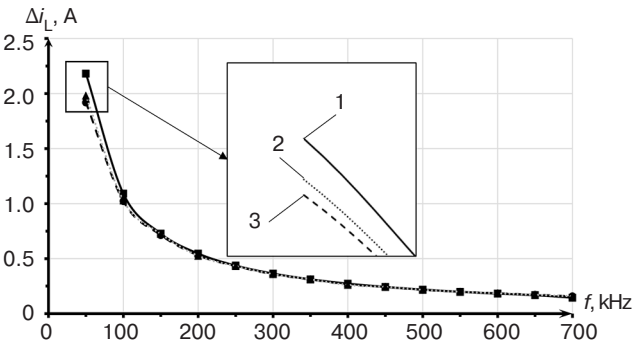

Fig. 7. Impact of switching frequency on ripple currents flowing through the winding of chokes L1 and L2 at the duty factor equal to 0.5: 1 is the calculated value Δi_L; 2 is the simulation result Δi_{L2m}; 3 is the simulation result Δi_{L1m}

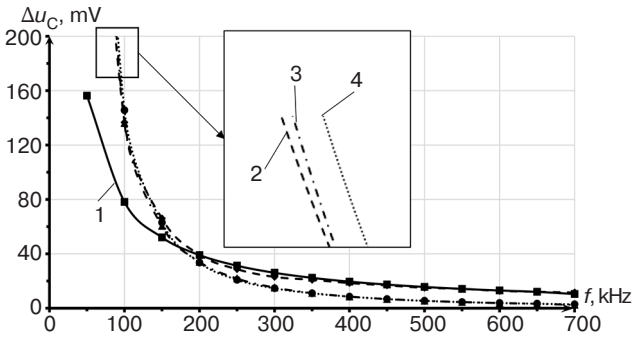

Fig. 8. Impact of switching frequency on the voltage on capacitors C1, C2 at the duty factor equal to 0.5: 1 is the calculated value Δu_{C1}; 2 is the simulation result Δu_{C1m}; 3 is the calculated value Δu_{C2}; 4 is the simulation result Δu_{C2m}

example, at the frequency of 100 kHz, the calculated value Δu_{C1} is 78 mV while simulation Δu_{C1} is 136 mV. The values of phase coordinates of the limiting continuous mathematical model tend to the values of currents and voltages of the converter at frequencies higher than 200 kHz. It can be seen from Fig. 8 that the calculated ripple and the simulated ripple coincide at frequencies higher than 200 kHz. The maximum difference is observed at ~230 kHz and is equal to ~3 mV for Δu_{C1} at Δu_{C1} = 31 mV. For ripples Δu_{C2}, the difference is ~0.9 mV at Δu_{C2} = 21.8 mV.

CONCLUSIONS

The present work presents equivalent circuits Zeta topology-based DC/DC converters in the modes of energy storage and transfer. Using Kirchhoff's rules, systems of equations describing each phase of the device are set up. In order to formulate the mathematical model in matrix form, the systems of equations are converted into a phase coordinate matrix, a coefficient matrix of phase coordinates, and a coefficient matrix of the external source. To permit the complete analysis of the limiting continuous mathematical model, equations for constant components are written.

Using the representation of currents and voltages as a sum of constant and variable components, systems of equations describing the converter in the modes of energy storage and transfer are written. Derived expressions of constant components of currents and voltages are integrated with systems of equations describing each phase and expressions for determining the ripple currents flowing through the winding of chokes and voltages on capacitors.

The results of ripple calculations when using the limiting continuous mathematical model and converter simulation are compared. The dependences of ripples on duty factor D and switching frequency of power switch f are obtained. At duty factor D = 0.5, the ripples obtained by the mathematical model coincide with those obtained by simulation. The difference is ~7 mA at Δi_L = 220 mA for ripple currents Δi_{L1}, Δi_{L2}. The difference between the voltage ripples is ~0.3 mV at Δu_{C1} = 15 mV for the Δu_{C1} ripple and ~0.05 mV at Δu_{C2} = 5.5 mV for the Δu_{C2} ripple. The maximum deviations of calculated values from simulation results at duty factor D = 0.8 are 47 mA for Δi_{L1} and Δi_{L2}, 76.4 mV for Δu_{C1}, and 1.59 mV for Δu_{C2}.

The presented limiting continuous mathematical model allows variation range of currents flowing through the choke windings and voltages at the coatings of the capacitor to be estimated along with their maximum and minimum values at different converter parameters such as switching frequency of the power switch, duty factor, nominal values of elements, etc. The obtained dependences can be used to rationally select electronic components for constructing Zeta topology converters.

Authors' contribution. All authors equally contributed to the research work.

REFERENCES

1. Bityukov V.K., Ivanov A.A., Mironov A.V., Mikhnevich N.G., Perfiliev V.S., Petrov V.A. Test bench for studying characteristics integrated circuit chips of secondary regulated charge pump power supply. *Russ. Technol. J.* 2016;4(3):37–52 (in Russ.). https://doi.org/10.32362/2500-316X-2016-4-3-37-52
2. Zakharov L.F. Pulsed voltage regulator with wide input voltage change limits. *Elektrosvyaz = The Elektrosvyaz Magazine*. 2018;11:81−82 (in Russ.).
3. Garelina S.A., Latyshenko K.P., Frunze A.V., Gorbunov R.A. Practical implementation of pyrometers for measuring flame temperature and objects through a flame. *Nauchnye i obrazovatel'nye problemy grazhdanskoi zashchity = Scientific and Educational Tasks of Civil Defence*. 2020;2(45):110–115 (in Russ.).
4. Odinokov A.O., Kremzukov Yu.A. Selecting DC converter topology. SEPIC or Zeta. *Prakticheskaya silovaya elektronika = Practical Power Electronics*. 2022;4(88):44–47 (in Russ.).
5. Vasyukov I.V., Pavlenko A.V., Batishchev D.V. Review and analysis of topologies of converters of power supply systems on hydrogen fuel cells for unmanned aerial vehicles of kilowatt power class. *Izvestiya vysshikh uchebnykh zavedenii. Elektromekhanika = Russian Electromechanics*. 2022;65(2):19–26 (in Russ.). https://doi.org/10.17213/0136-3360-2022-2-19-26
6. Choudhary V. Transient resistant primary DC/DC converter solutions for automotive electronics power systems. *Silovaya elektronika = Power Electronics*. 2017;3(66):30–34 (in Russ.). Available from URL: https://power-e.ru/wp-content/uploads/6630.pdf
7. Kazantsev D.P., Shcherbak V.F., Zakamaldin D.A., Kazantsev Yu.E., Pronin A.V., Molodykh S.V. *Electric Cardiac Pacemaker*: RF Pat. 2531695. Publ. 27.10.2014 (in Russ.).
8. Kastrov M.Yu., Makarov V.V. Zeta converter based on SIPEX SP16125/6/7 controllers design baseline. *Prakticheskaya silovaya elektronika = Practical Power Electronics*. 2010;2(38):15–18 (in Russ.).
9. Korshunov A.I. Methodology for constructing continuous models of pulsed DC voltage converters. *Komponenty i tekhnologii = Components & Technologies*. 2006;8(61):124−130 (in Russ.). Available from URL: https://kit-e.ru/powerel/metodika-postroeniya-nepreryvnyh-modelej-impulsnyh-preobrazovatelej-napryazheniya-postoyannogo-toka/
10. Bityukov V.K., Simachkov D.S., Babenko V.P. *Istochniki vtorichnogo elektropitaniya* (*Secondary Power Sources*). Moscow: Infra-Inzheneriya; 2020. 376 p. (in Russ.).
11. Erickson R.W., Maksimović D. *Fundamentals of Power Electronics*. NY: Springer; 2020. 1084 p. https://doi.org/10.1007/978-3-030-43881-4
12. Jozwik J.J., Kazimierczuk M.K. Dual Sepic PWM Switching-Mode DC/DC Power Converter. *IEEE Transactions on Industrial Electronics*. 1989;36(1):64–70. https://doi.org/10.1109/41.20346

СПИСОК ЛИТЕРАТУРЫ

1. Битюков В.К., Иванов А.А., Миронов А.В., Михневич Н.Г., Перфильев В.С., Петров В.А. Стенд для исследования характеристик микросхем источников вторичного электропитания с накачкой заряда. *Russ. Technol. J.* 2016;4(3):37–52. https://doi.org/10.32362/2500-316X-2016-4-3-37-52
2. Захаров Л.Ф. Импульсный стабилизатор напряжения с широкими пределами изменения входного напряжения. *Электросвязь*. 2018;11:81−82.
3. Гарелина С.А., Латышенко К.П., Фрунзе А.В., Горбунов Р.А. Практическая реализация пирометров для измерения температуры пламени и объектов сквозь пламя. *Научные и образовательные проблемы гражданской защиты*. 2020;2(45):110–115.
4. Одиноков А.О., Кремзуков Ю.А. Выбор топологии преобразователя постоянного напряжения. SEPIC или Zeta. *Практическая силовая электроника*. 2022;4(88):44–47.
5. Васюков И.В., Павленко А.В., Батищев Д.В. Обзор и анализ топологий преобразователей систем электропитания на водородных топливных элементах для беспилотных летательных аппаратов киловаттного класса мощности. *Известия ВУЗов. Электромеханика*. 2022;65(2):19–26. https://doi.org/10.17213/0136-3360-2022-2-19-26
6. Чоудхари В. Решения устойчивого к переходным процессам первичного DC/DC-преобразователя системы питания автомобильной электроники. *Силовая электроника*. 2017;3(66):30–34. URL: https://power-e.ru/wp-content/uploads/6630.pdf
7. Казанцев Д.П., Щербак В.Ф., Закамалдин Д.А., Казанцев Ю.Е., Пронин А.В., Молодых С.В. *Оптико-электронный аппарат*: пат. 2531695 РФ. Заявка № 2012156979/14; заявл. 24.12.2012; опубл. 27.10.2014. Бюл. № 30.
8. Кастров М.Ю., Макаров В.В. Основы разработки преобразователя Zeta на базе контроллеров SIPEX SP16125/6/7. *Практическая силовая электроника*. 2010;2(38):15–18.
9. Коршунов А.И. Методика построения непрерывных моделей импульсных преобразователей напряжения постоянного тока. *Компоненты и технологии*. 2006;8(61):124−130. URL: https://kit-e.ru/powerel/metodika-postroeniya-nepreryvnyh-modelej-impulsnyh-preobrazovatelej-napryazheniya-postoyannogo-toka/
10. Битюков В.К., Симачков Д.С., Бабенко В.П. *Источники вторичного электропитания*. М.: Инфра-Инженерия; 2020. 376 с.
11. Erickson R.W., Maksimović D. *Fundamentals of Power Electronics*. NY: Springer; 2020. 1084 p. https://doi.org/10.1007/978-3-030-43881-4
12. Jozwik J.J., Kazimierczuk M.K. Dual Sepic PWM Switching-Mode DC/DC Power Converter. *IEEE Transactions on Industrial Electronics*. 1989;36(1):64–70. https://doi.org/10.1109/41.20346
13. Пономарев Ю.Г., Присмотров Н.И., Шураков И.А. Вентильный электропривод с высоким коэффициентом мощности. *Интеллектуальная электротехника*. 2022;1(17):27–41. https://doi.org/10.46960/2658-6754_2022_1_27

13. Ponomarev Yu.G., Prismotrov N.I., Shurakov I.A. BLDC and PMBLAC motor drives with high power factor. *Intellektual'naya elektrotekhnika = Smart Electrical Engineering*. 2022;1(17):27–41 (in Russ.). https://doi.org/10.46960/2658-6754_2022_1_27
14. Korshunov A.I. Limiting continuous model of a system with high-frequency structure variation. *Izvestiya vysshikh uchebnykh zavedenii. Priborostroenie = J. Instrument Eng.* 2009;52(9):42−48 (in Russ.). Available from URL: https://pribor.ifmo.ru/file/article/4902.pdf
15. Korshunov A.I. Limiting continuous model of a system with periodic high-frequency structure variation. *Silovaya elektronika = Power Electronics*. 2021;5(92):48−51 (in Russ.).
16. Korshunov A.I. Improving the quality of output voltage stabilisation of a pulsed DC converter. *Izvestiya vysshikh uchebnykh zavedenii. Priborostroenie = J. Instrument Eng.* 2013;56(3):48−57 (in Russ.). Available from URL: https://pribor.ifmo.ru/file/article/6176.pdf
17. Korshunov A.I. Two approaches to stability analysis of DC-DC converters with variable structure of power stage. *Prakticheskaya silovaya elektronika = Practical Power Electronics*. 2017;2(66):12−19 (in Russ.).
18. Korshunov A.I. Pulsed DC voltage converter based on Chuk scheme. *Silovaya elektronika = Power Electronics*. 2017;4(67):60−66 (in Russ.).
19. Korshunov A.I. Specifics of DC voltage stabilization by Chuk converter. *Prakticheskaya silovaya elektronika = Practical Power Electronics*. 2017;4(68):2−9 (in Russ.).
20. Bityukov V.K., Lavrenov A.I. Mathematical model of a DC/DC voltage converter based on Zeta topology. In: *Fundamental, Prospecting, Applied Research and Innovative Projects*: *Proceedings of the National Scientific and Practical Conference.* Moscow: RTU MIREA; 2022. P. 209−215 (in Russ.).
21. Bityukov V.K., Lavrenov A.I., Malitskiy D.A. Mathematical model of DC/DC converter based on Zeta topology (Part 1). *Proektirovanie i tekhnologiya elektronnykh sredstv = Design and Technology of Electronic Means*. 2022;4:53−57 (in Russ.).
22. Bityukov V.K., Lavrenov A.I., Malitskiy D.A. Mathematical model of DC/DC converter based on Zeta topology (Part 2). *Proektirovanie i tekhnologiya elektronnykh sredstv = Design and Technology of Electronic Means*. 2023;1:48−53 (in Russ.).
23. Babenko V.P., Bityukov V.K. Simulation of Switching of High-Power FETs Using the Electronics Workbench Software. *J. Commun. Technol. Electron.* 2019;64(2): 176–181. https://doi.org/10.1134/S1064226919020025 [Original Russian Text: Babenko V.P., Bityukov V.K. Simulation of Switching of High-Power FETs Using the Electronics Workbench Software. *Radiotekhnika i elektronika = J. Commun. Technol. Electron.* 2019;64(2):199−205 (in Russ.). https://doi.org/10.1134/S0033849419020025]
24. Babenko V.P., Bityukov V.K., Kuznetsov V.V., Simachkov D.S. Simulation of static and dynamic losses in MOSFET keys. *Russ. Technol. J.* 2018;6(1):20−39 (in Russ.). https://doi.org/10.32362/2500-316X-2018-6-1-20-39
14. Коршунов А.И. Предельная непрерывная модель системы с высокочастотным периодическим изменением структуры. *Известия ВУЗов. Приборостроение*. 2009;52(9):42−48. URL: https://pribor.ifmo.ru/file/article/4902.pdf
15. Коршунов А.И. Предельная непрерывная модель системы с периодическим высокочастотным изменением структуры. *Силовая электроника*. 2021;5(92):48−51.
16. Коршунов А.И. Повышение качества стабилизации выходного напряжения импульсного преобразователя постоянного тока. *Известия ВУЗов. Приборостроение*. 2013;56(3):48−57. URL: https://pribor.ifmo.ru/file/article/6176.pdf
17. Коршунов А.И. Два подхода к анализу устойчивости стабилизаторов напряжения постоянного тока с переменной структурой силовой части. *Практическая силовая электроника*. 2017;66:12−19.
18. Коршунов А.И. Импульсный преобразователь напряжения постоянного тока по схеме Чука. *Силовая электроника*. 2017;4(67):60−66.
19. Коршунов А.И. Особенности стабилизации напряжения постоянного тока с помощью преобразователя Чука. *Практическая силовая электроника*. 2017;4(68):2−9.
20. Битюков В.К., Лавренов А.И. Математическая модель DC/DC преобразователя напряжения, построенного по Zeta топологии. *Фундаментальные, поисковые, прикладные исследования и инновационные проекты: сборник трудов Национальной научно-практической конференции*; под ред. С.У. Увайсова. М.: РТУ МИРЭА; 2022. С. 209−215.
21. Битюков В.К., Лавренов А.И., Малицкий Д.А. Математическая модель DC/DC преобразователя, построенного по Zeta топологии (часть 1). *Проектирование и технология электронных средств*. 2022;4:53−57.
22. Битюков В.К., Лавренов А.И., Малицкий Д.А. Математическая модель DC/DC преобразователя, построенного по Zeta топологии (часть 2). *Проектирование и технология электронных средств*. 2023;1:48−53.
23. Бабенко В.П., Битюков В.К. Имитационное моделирование процессов переключения силовых полевых транзисторов в программе Electronics Workbench. *Радиотехника и электроника*. 2019;64(2):199−205. https://doi.org/10.1134/S0033849419020025
24. Бабенко В.П., Битюков В.К., Кузнецов В.В., Симачков Д.С. Моделирование статических и динамических потерь в MOSFET ключах. *Russ. Technol. J.* 2018;6(1):20−39. https://doi.org/10.32362/2500-316X-2018-6-1-20-39

About the authors

Vladimir K. Bityukov, Dr. Sci. (Eng.), Professor, Department of Radio Wave Processes and Technology, Institute of Radio Electronics and Informatics, MIREA – Russian Technological University (78, Vernadskogo pr., Moscow, 119454 Russia). E-mail: bitukov@mirea.ru. ResearcherID Y-8325-2018, Scopus Author ID 6603797260, RSCI SPIN-code 3834-5360, https://orcid.org/0000-0001-6448-8509

Alexey I. Lavrenov, Assistant, Department of Radio Wave Processes and Technology, Institute of Radio Electronics and Informatics, MIREA – Russian Technological University (78, Vernadskogo pr., Moscow, 119454 Russia). E-mail: lavrenov@mirea.ru. SPIN-код РИНЦ 6048-5027, https://orcid.org/0000-0001-5722-541X

Daniil A. Malitskiy, Assistant, Department of Radio Wave Processes and Technology, Institute of Radio Electronics and Informatics, MIREA – Russian Technological University (78, Vernadskogo pr., Moscow, 119454 Russia). E-mail: malickij@mirea.ru. SPIN-код РИНЦ 4912-3018, https://orcid.org/0000-0003-4558-9085

Об авторах

Битюков Владимир Ксенофонтович, д.т.н., профессор, кафедра радиоволновых процессов и технологий Института радиоэлектроники и информатики ФГБОУ ВО «МИРЭА – Российский технологический университет» (119454, Россия, Москва, пр-т Вернадского, д. 78). E-mail: bitukov@mirea.ru. ResearcherID Y-8325-2018, Scopus Author ID 6603797260, SPIN-код РИНЦ 3834-5360, https://orcid.org/0000-0001-6448-8509

Лавренов Алексей Игоревич, ассистент, кафедра радиоволновых процессов и технологий Института радиоэлектроники и информатики ФГБОУ ВО «МИРЭА – Российский технологический университет» (119454, Россия, Москва, пр-т Вернадского, д. 78). E-mail: lavrenov@mirea.ru. SPIN-код РИНЦ 6048-5027, https://orcid.org/0000-0001-5722-541X

Малицкий Даниил Александрович, ассистент, кафедра радиоволновых процессов и технологий Института радиоэлектроники и информатики ФГБОУ ВО «МИРЭА – Российский технологический университет» (119454, Россия, Москва, пр-т Вернадского, д. 78). E-mail: malickij@mirea.ru. SPIN-код РИНЦ 4912-3018, https://orcid.org/0000-0003-4558-9085

Translated from Russian into English by Kirill V. Nazarov
Edited for English language and spelling by Thomas A. Beavitt